SIMCor

In-Silico testing and validation of Cardiovascular IMplantable devices

Call: H2020-SC1-DTH-2018-2020 (*Digital transformation in Health and Care*)

Topic: SC1-DTH-06-2020 (*Accelerating the uptake of computer simulations for testing medicines and medical devices*)

Grant agreement No: 101017578

Deliverable 8.5

Fast device deployment model

Due date of delivery: 31 December 2022

Actual submission date: 22 December 2022

Start of the project: 1 January 2021
End date: 31 December 2023

This project has received funding from the European Union's Horizon 2020 research and innovation programmeunder grant agreement N° 101017578

Reference

Name	SIMCor_D8.5_ Fast device deployment model _CHA_22-12-2022
Lead beneficiary	Charité – Universitätsmedizin Berlin (CHA)
Author(s)	Lars Walczak (CHA)
Dissemination level	Public
Type	Report
Official delivery date	31 December 2022
Date of validation by the WP Leader	12 December 2022
Date of validation by the Coordinator	**22 December 2022**
Signature of the Coordinator	

Version log

Issue date	Version	Involved	Comments
25/11/2022	1.0	Lars Walczak (CHA)	First draft by CHA
12/12/2022	2.0	Andreas Arndt (BIO)	Internal review by BIO
13/12/2022	3.0	Jan Brüning (CHA)	Project Coordinator's review
21/12/2022	4.0	Anna Rizzo (LYN)	Final review and formal checking by LYN
22/12/2022	Final	Jan Brüning (CHA)	Submission by PC

Executive summary

In this document, we report the results of *T8.4 - Fast device deployment modelling*. The goal of this task is to develop computationally efficient, physics-based models for simulation of device deployment and implement a prototype for the SIMCor use cases of PAPS and TAVI. The approach has to maintain an appropriate level of accuracy while simultaneously reducing the model complexity and numerical costs in comparison to the high-fidelity finite element approaches, such as the simulation model described in *D8.6 - Report on 3D finite element simulation (PHI, M24)*. Only simplified parameterization as well as simple geometric anatomy and device representations are required. Such a simplified parameterization reduces preparation as well as simulation time and facilitates the automated processing of a large cohort. It enables interactive and automatic placement, e.g., regarding the orientation or angulation of devices inside a vessel.

Table of contents

List of figures

Acronyms

Acronym	Full name
AS	Aortic stenosis
AVR	Aortic valve replacement
CFD	Computational fluid dynamics
FE	Finite element
FEM	Finite element method
LVOT	Left ventricular outflow tract
PA	Pulmonary artery
PAP	Pulmonary artery pressure
PAPS	Pulmonary artery pressure sensor
PBD	Position-based dynamics
RANS	Reynolds-Averaged Navier-Stokes
SAVR	Surgical aortic valve replacement
TAVI	Transcatheter aortic valve implantation
TAVR	Transcatheter aortic valve replacement
TPG	Transvalvular pressure gradient

Introduction

As input for the methods developed and evaluated in T8.4, we used 3D triangular mesh representations for the anatomical compartments, as defined in *T6.1 - Processing pipeline and database concept for TAVI and PAPS*, and multiple 3D device models, such as reverse-engineered aortic valve prosthesis models as well as PAPS models provided by BIO in *T8.1 - Device model enhancement*. Generalized assumptions on tissue elasticity were derived from literature or the model parameters described, e.g., in for the deliverables *D8.3 - Constitutive vessel model (TUG, M20)*. The device implant was considered as being rigid, meaning that the device itself could not deform. Thus, only rigid body motion of the device and subsequently interaction with the elastic vessel wall, such as during device expansion or device movement, were possible. In contrast, the more complex models developed and evaluated in *T8.5 - 3D finite element implant simulation allow deformation of the device, as for example the TAVI stent frame or the fixation wires of the PAPS*. Using *position-based dynamics* (PBD), which is a mass-constraint system, spring connections and contact conditions for devices were defined by additional constraints. The approach resulted in a deformed 3D vessel geometry for further analysis in WP8 and WP9. An initial validation of the fast device deployment method was performed based on detailed implant simulations using the FE model described in *D8.1 - PAPS model (BIO, M12)* as well as additional measurements from clinical routine collected in WP5 and processed in WP6.

Aortic valve replacement

In *aortic valve replacement* (AVR), the treatment strategy, the model and the size of the implanted prosthesis have a major impact on the postoperative hemodynamics and, thus, on the clinical outcome. Pre-clinical cohort-sized *computational fluid dynamics* (CFD) studies could help developing improved device designs as well as improve our understanding of aorta hemodynamics and the interaction with implants. Pre-interventional prediction of the post-interventional hemodynamics could support the treatment decision. For this, efficient methods are needed for the analysis of large cohorts and for prediction of patient-individual outcomes.

In Walczak et al.[1], we presented a novel approach using *position-based dynamics* (PBD) to simulate deformation in aortic valve replacement scenarios with applications in surgical or interventional planning and batch domain creation for computational fluid dynamics studies investigating aortic hemodynamics in large samples. To place and orient the device in the aorta, we used a centreline-based approach. Points on the centreline were used for placement while centreline tangent vectors we used for orientation along the centreline as well as angulation and placement relative to the plane defined by the tangent. Ray casting was used to define springs connecting the device to the aortic wall and, thus, modelling virtual surgical implantations. Setting the rest length of the springs to zero, we induced deformation of the aorta moving towards the device. In addition, the device could expand during this process. After deformation, both the aortic and the device mesh could manually be combined into a single mesh for use in subsequent CFD models.

For SIMCor, we extended the simulation approach described above. Rigid body movement of the valve prosthesis and two-sided interaction between device and vessel wall in the landing zone could be modelled. In addition, we modified the mesh generation operations and implemented additional methods for refining or deleting mesh elements in order to create a fully automated, high-quality boundary mesh. This boundary description consisted of a combined, single mesh that could directly be used for generating a volumetric mesh suitable for computational fluid dynamics in an external tool such as STAR-CCM+. This greatly reduced the time needed to prepare the boundary mesh representation compared to manual or semi-automatic procedures used before. Generation of a single boundary description with approximately 100k surface elements using this implantation simulation approach required approximately 3 minutes to complete and made this approach applicable to analysing large datasets.

The PBD-based boundary mesh generation method was applied in Franke et al.[2] in a first larger computational study. In this study, we performed virtual treatment with *transcatheter* AVR (TAVI) and biological *surgical* AVR (SAVR) and compared hemodynamic outcomes using numerical simulations. 10 patient cases with severe *aortic stenosis* (AS) undergoing TAVI were virtually treated with both biological SAVR and TAVI to compare post-interventional hemodynamics using numerical simulations of peak-systolic flow. We applied the method to the patient's anatomy including *left ventricular outflow tract* (LVOT), aortic root and aorta. Geometries were automatically reconstructed from dynamic CT-scans and patient-specific flow rates were calculated by volumetric analysis of the left ventricle. Hemodynamics were calculated using STAR-CCM+ by solving the *Reynolds-Averaged Navier-Stokes* (RANS) equations.

Evaluation of the results was performed using echocardiographic measurements of the real post-procedural outcome. Virtual treatment with TAVI resulted in realistic hemodynamics comparable to

[1] Walczak, L, Goubergrits, L, Hüllebrand, M, Georgii, J, Falk, V and Hennemuth, A. "Using position-based dynamics to simulate deformation in aortic valve replacement procedure" *Current Directions in Biomedical Engineering*, vol. 6, no. 1, 2020, pp. 20200042. https://doi.org/10.1515/cdbme-2020-0042

[2] [2] Franke, B, Schlief, A, Walczak, L, Sündermann, S, Unbehaun, A, Kempfert, J, et al. Comparison of hemodynamics in biological surgical aortic valve replacement and transcatheter aortic valve implantation—An in-silico study. Artif. Organs. 2022; 00: 1– 9. https://doi.org/10.1111/aor.14405

echocardiographic measurements (median difference in *transvalvular pressure gradient* (TPG): −0.33 mm Hg). Virtual TAVI and SAVR showed similar hemodynamic function with a mean TPG with standard deviation of 8.45 ± 4.60 mm Hg in TAVI and 6.66 ± 3.79 mm Hg in SAVR (p = 0.03) while max. wall shear stress being 12.6 ± 4.59 vs. 10.2 ± 4.42 Pa (p = 0.001). TAVI and SAVR show similar hemodynamics in a pairwise comparison.

Using the PBD-based method for virtual treatment, we were able to reliably predict post-interventional hemodynamics. *Figure 1* and *Figure 2* show an exemplary AVR dataset in which the valve model was fixed or was able to move in the landing zone after placement. Based on the results of this initial validation study, the method pipeline is now ready to be applied to models generated based on the virtual cohort in WP8 and WP9. Overall, the time to prepare datasets is greatly reduced by the automated approach.

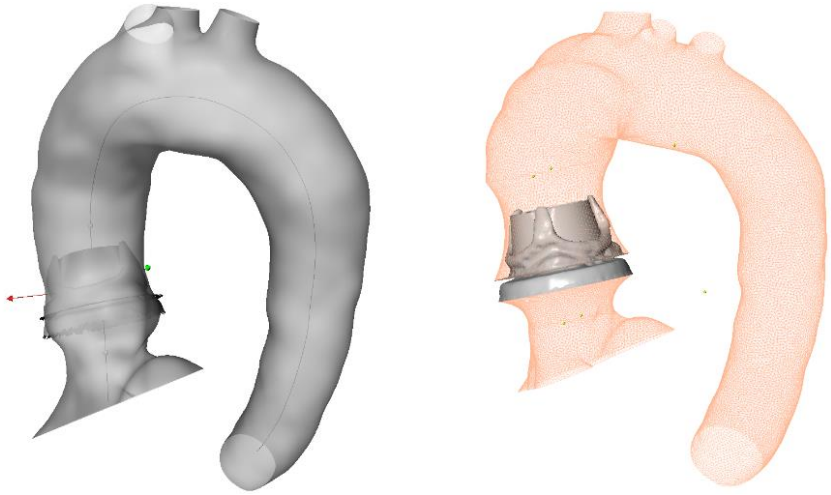

Figure 1: Left: Exemplary placement of device inside the aortic root. Note that the valve in too large to fit inside the aorta. The faint black line inside the aorta depicts the centreline. Right: Simulation result and combined boundary mesh. The valve was held fixed inside the landing zone and deformed the aortic wall accordingly.

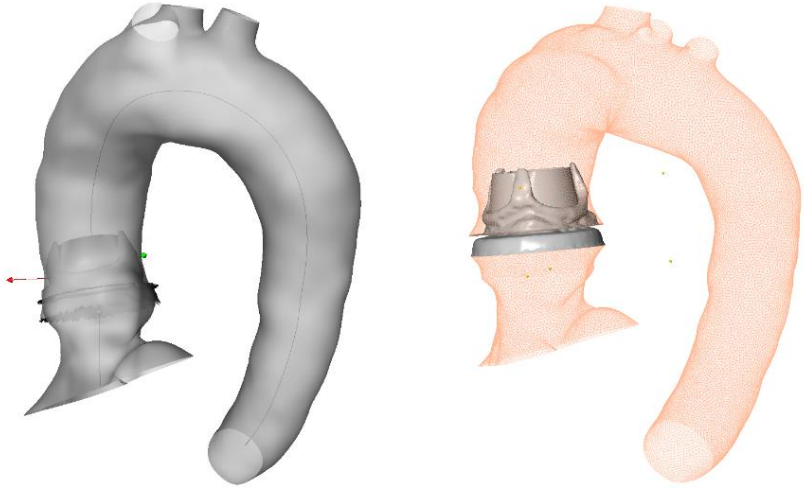

Figure 2: Left: Exemplary placement of device inside the aortic root (see above). Right: Simulation result and combined boundary mesh. The valve was allowed to undergo rigid body motion inside the landing zone and two-way interact with the aortic wall. This results in a different angulation of the device inside the vessel compared with the case in which the valve was fixed in place.

PAPS device placement

Based on the PBD simulation engine used for AVR, we developed methods for simulating PAPS placement. We evaluated two approaches with different degree of complexity in the PAPS model (see *D8.1 – PAPS model (BIO, M12)*, 'PAPS structural features' section). The first one included the proximal and distal fixation elements of the sensor in their initial configuration (without crimping and expansion) while the second approach neglected explicit modelling of the fixation elements. Instead, the forces applied by fixation elements were used to push the sensor body into the vessel wall. The forces were based on the analysis of the forces calculated in FE results described in D8.1, 'Simulation of the release step in an artificial artery' section, but had to be rescaled in order to fit to the PBD approach. The first approach used an expansion of the full device model (including the fixation elements) to push the sensor into the vessel wall. Material parameters for the *pulmonary artery* (PA) were set to comparable values for the Young's modulus described in D8.1, 'Vessel and surrounding lung tissue material model' section. Device placement resembled the approach taken in the AVR case since it used the centreline information created in WP6 to place and orient the sensor inside of different branches of the PA.

We compared the results of the PAPS placement with fixation elements to results obtained using the FE approach in D8.1 and found the deformation to be over-estimated by the PBD simulation. This could not be attributed to differences in the initial positions of the sensor but were clearly related to the simplified modelling. The rigid fixation elements used in their initial configuration pushed the opposite vessel wall too far outwards compared to the results based on the FE model described in D8.1. The approach therefore was discarded because it produced unrealistically large deformations (using the initial fixation element size). The results are depicted in *Figure 3* and *Figure 4*, showing the results and a visual comparison with the FE results.

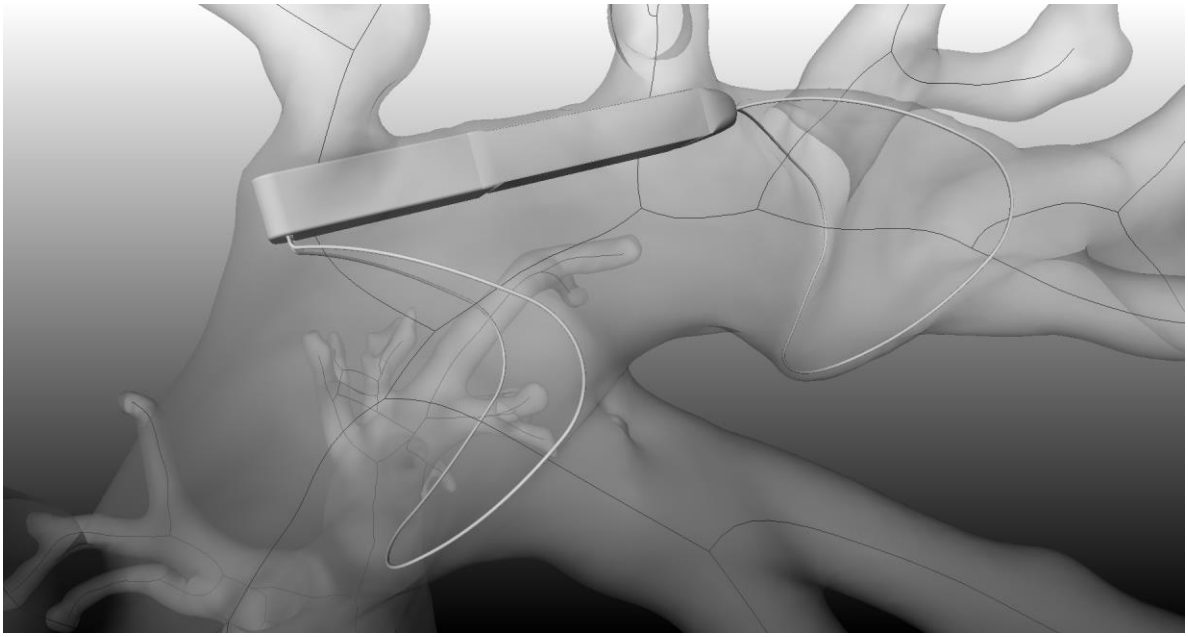

Figure 3: Simulation result including the sensor's fixation elements. The sensor is displayed in grey and is pushed into the vessel wall. The deformed pulmonary artery is shown in grey and exhibits large deformations at the vessel wall opposite to the sensor body because of the rigid fixation elements. The centreline used for placement is depicted as a tree structure (black lines).

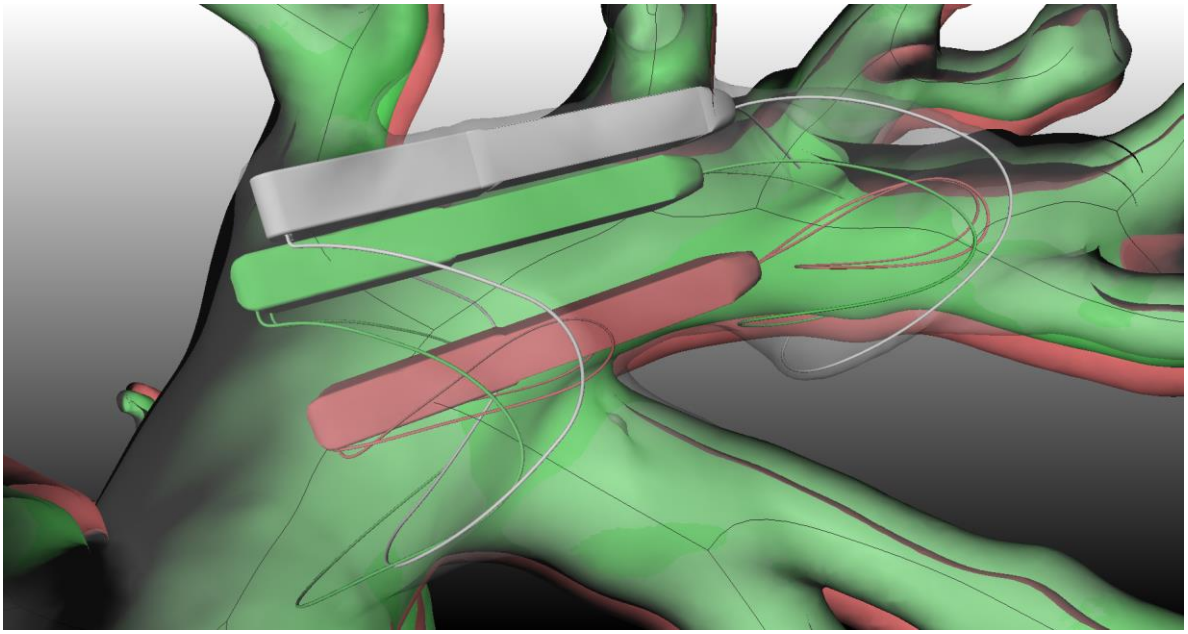

Figure 4: Different results are displayed on top of each other. The results of the FE simulation performed analogue to D8.1 (red: initial position, green: expanded) are shown compared to the PBD results shown in Fig. 1, i.e., using the rigid fixation elements during simulated expansion. The deformation is over-estimated by the simplified approach because of the rigid fixation elements. The sensor is pushed too far outwards, and the opposite vessel wall exhibits a too large deformation.

Instead of explicit modelling, we only used the geometry of the sensor body and replaced the fixation elements using a force-based approach. The results obtained with this approach did not deform the vessel wall opposite to the sensor, but since the deformation was not that large to begin with based on the FE results, it was considered to not have significant enough influence on CFD simulation results and, therefore, it was considered acceptable to neglect the influence of the fixation elements to the opposite vessel wall for the fast device placement step.

Figure 5 shows a qualitative comparison with the FE results. Results were not directly comparable because of the different initial positions of the sensor. As in the FE model, the deployment of the fixation elements was modelled, different configurations of the fixation elements compared to the PBD model were observed. Most importantly, the proximal fixation element was expanding and finally anchoring in a side branch, which was not possible to model using the PBD approach. However, the results underline the complexity of the modelling effort in real world geometries with respect to simple tube geometries. In addition, these results show potential future refinements in the modelling of the PBD case. *Figure 5* also shows an asymmetric expansion of the fixation elements in the FE results. This could be modelled by applying different force magnitudes and directions to the sensor (distal and proximal) in the PBD rigid body simulation.

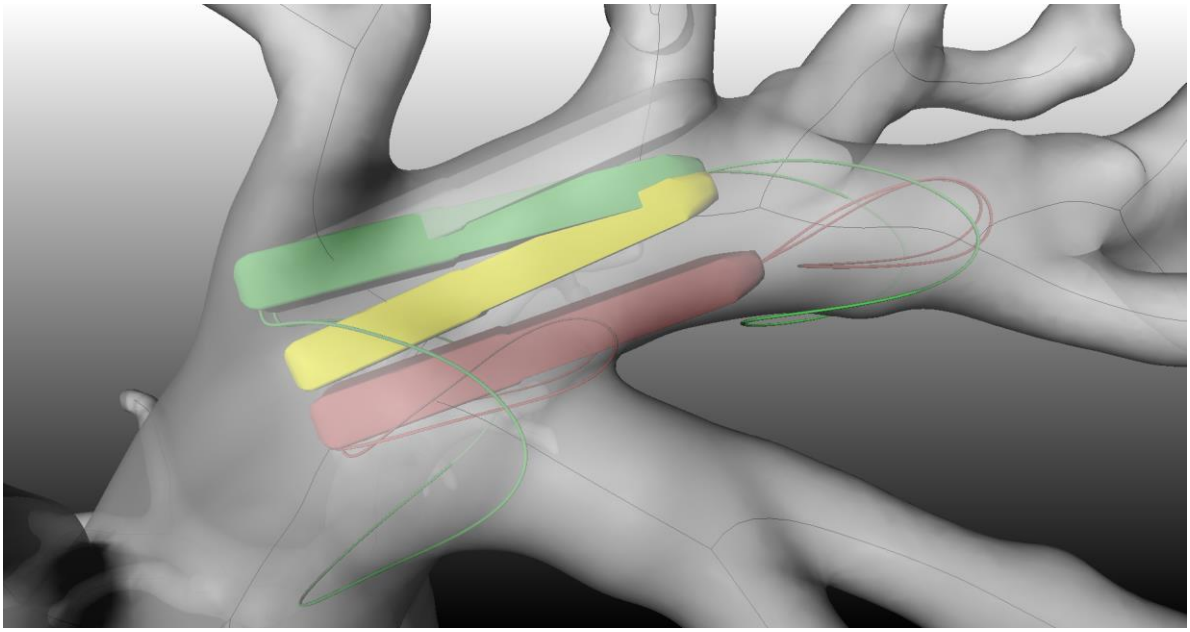

Figure 5: The second simulation approach without fixation elements provided an improved result since the sensor was pushed into the vessel wall but did not deform the opposite vessel wall with the rigid fixation elements. Here, a comparison between FE and PBD result are shown (FE: green, PBD: grey). Because of the differences in the initial placement and expansion of the distal fixation element (red: FE, sensor placed on opposite wall, yellow: PBD, sensor placed at centreline), the results differ in their final positions. The FE model did not reach the final position due to interaction with the side branches).

Using the PA segmentation and centreline extraction methods developed in WP6, we can batch-process all data sets created in WP6 and WP7 using a sensor body model. *Figure 6* and *Figure 7* show exemplary simulation results from inside and outside of an exemplary PA model. Like the AVR case, the sensor can be angulated along the centreline tangent, such that the backside of the sensor is pushed into the vessel wall as desired. The results resemble the rotation of the crimped sensor around the long axis and expansion of the fixation elements neglecting the expansion complexity. A single simulation using up to 200k triangles to represent the full vessel, and sensor takes about 3 min to complete on a current notebook system.

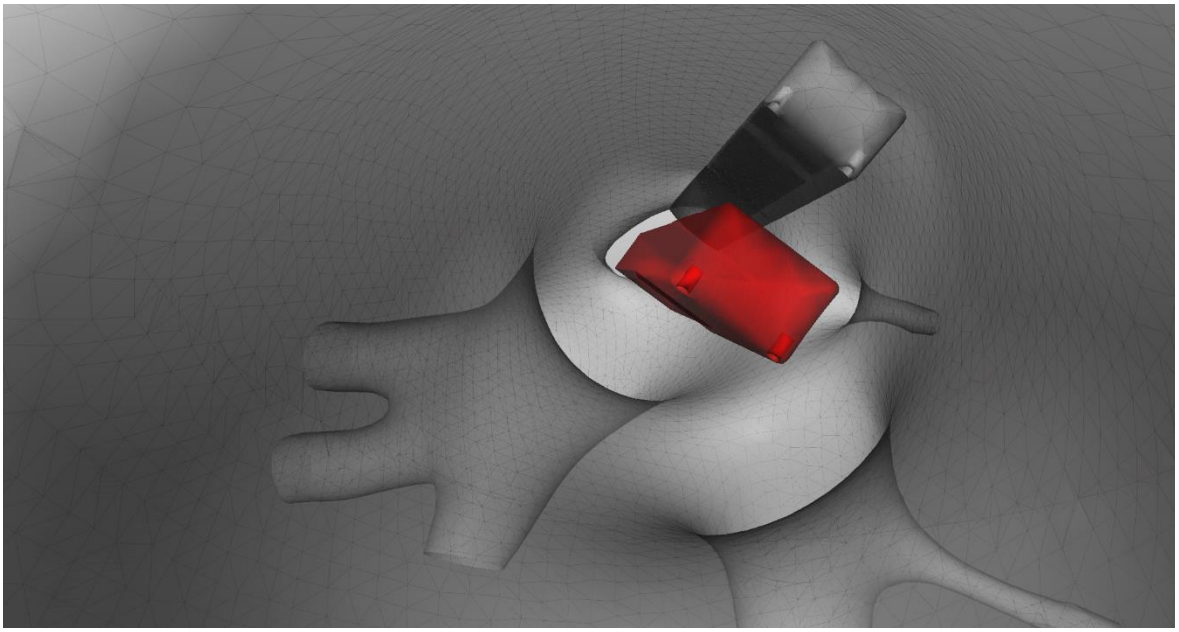

Figure 6: PBD simulation results for PAPS placement. Red: initial sensor position and orientation. Grey: Final position of sensor and deformed vessel. View from inside the PA.

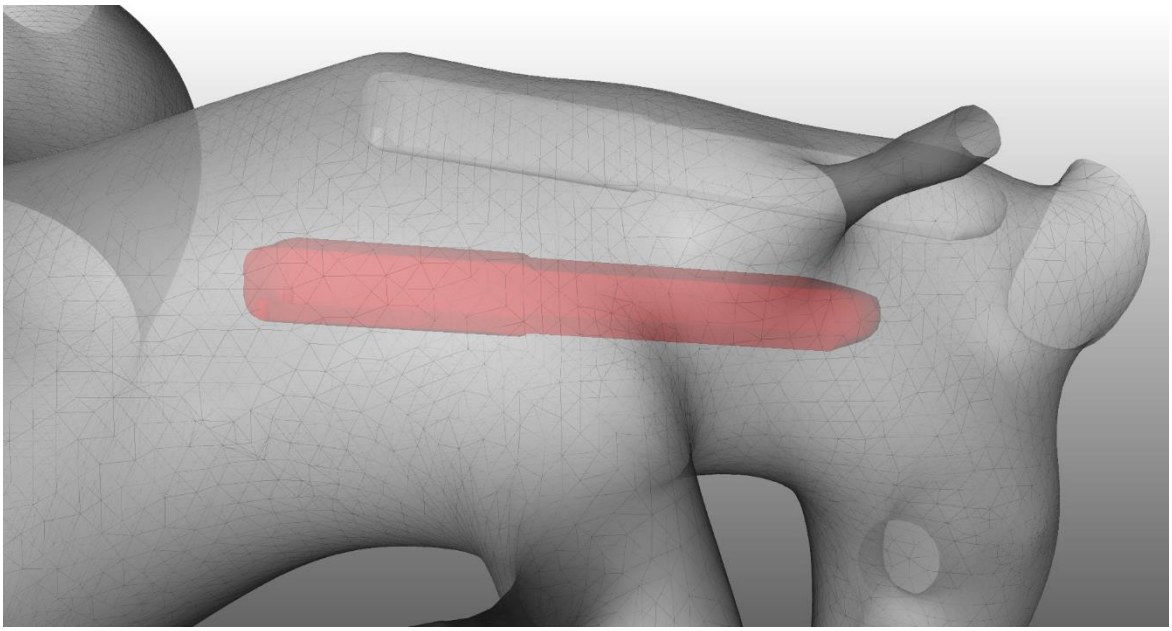

Figure 7: PBD simulation results for PAPS placement. Red: initial sensor position and orientation. Grey: Final position of sensor and deformed vessel. View from outside the PA.

Conclusion

After the initial positive evaluation of results, the methods developed in T8.4 are considered suitable for fast device deployment modelling of rigid-body and expanding rigid-body implants and can be used for batch-processing of large cohorts. For CFD simulations, only the final position of the (expanded) implant relative to the vessel wall is of interest. Based on results, we are able to conduct large cohort sized CFD studies in the AVR and PAPS cases in WP8 and 9. However, the current PBD simulation cannot model the interaction of deformable fixation elements (PAPS) or structures of a stent (TAVI) with the vessel wall. Hence, the current PBD model cannot be used to simulate device deployment when the final geometry of the implant is not prescribed but is dependent on the interaction between deformable vessel and deformable device fixation.